ACS APPLIED MATERIALS & INTERFACES

Research Article

www.acsami.org

Novel 3D Hierarchical Cotton-Candy-Like CuO: Surfactant-Free Solvothermal Synthesis and Application in As(III) Removal

Xin-Yao Yu,[†,§] Ren-Xia Xu,[†,‡,§] Chao Gao,[†,‡] Tao Luo,[†] Yong Jia,[†] Jin-Huai Liu,[†] and Xing-Jiu Huang*[,†,‡]

[†]Research Center for Biomimetic Functional Materials and Sensing Devices, Institute of Intelligent Machines, Chinese Academy of Sciences, Hefei, 230031, P.R. China

[‡]Department of Chemistry, University of Science and Technology of China, Hefei, 230026, P.R. China

Supporting Information

ABSTRACT: Novel three-dimensional (3D) hierarchical cotton-candy-like CuO microspheres were synthesized by a facile precursor templated conversion method. The precursor was prepared by solvothermal method in ethylene glycol (EG) without the use of any surfactant. The possible formation mechanism of the precursor was proposed and it was found that the synthetic parameters for the precursor such as the ratio of Cu^{2+} to urea, the reaction temperature, and the use of EG are crucial for the formation of the cotton-candy-like CuO precursor nanostructures. The cotton-candy-like CuO obtained by calcination were used as an adsorbent for removing As(III) in water. The adsorption isotherm, adsorption kinetics, the effects of competing anions and pH, and the adsorption mechanism were also investigated.

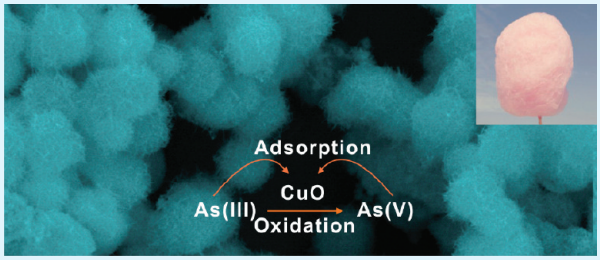

KEYWORDS: *cotton-candy-like CuO, solvothermal, hierarchical, nanostructures, adsorption, As(III)*

1. INTRODUCTION

Recent research has shown that the properties of materials depend largely on their particle size, morphology and structure.[1−6] It is expected that materials with novel morphologies and microstructures could exhibit effective and interesting functions. Over the past decades, three-dimensional (3D) hierarchical architectures comprised of nanofibers, nanoplates and nanobelts as primary building blocks have attracted great interests because of their unique structures and properties.[7−15] The synergistic effect of their nanometer-sized primary building blocks and overall micrometer-sized structure may be desirable for a variety of applications especially in water purification. Their overall micrometer-sized structure provides desirable mechanical strength, facile transportation, and easy recovery and their nanometer-sized primary building blocks provide a high surface area, a high surface-to-bulk ratio and enough surface active sites which can interact with micropollutants in water, e.g., heavy metal ions and organic micropollutants.[2,16−25]

Arsenic contamination in natural water poses a great threat to millions of people in many regions of the world such as China, Chile, India, Taiwan, USA, Argentina, Poland, Canada, Japan, New Zealand, Hungary, and Mexico.[26,27] Long-term drinking water exposure causes skin, lung, bladder, and kidney cancers.[27] The predominant forms of arsenic in groundwater and surface water are the inorganic species arsenate As(V) and arsenite As(III).[28] It has been recognized that As(III) is more prevalent in groundwater than was previously understood, which is of concern as it is more toxic than As(V).[29] Among various arsenic removal techniques, adsorption is believed to be a cost-effective and simple method.[27] As(III) is generally reported to have low affinity to the surface of various adsorbents compared with As(V).[30,31] Thus, a pretreatment process of As(III) by oxidizing it to As(V) before the adsorption process is necessary. So it is desirable to develop an effective adsorbent for As(III) without the oxidation process which could largely simplify the treatment procedure and lower the treatment cost. 3D hierarchically structured Fe_2O_3, Fe_3O_4 and CeO_2 have been used for adsorption of arsenic from water.[16,18,22,24] However, most of these studies focused on the removal of As(V) which is less toxic and relatively easier to remove. Therefore, there is an urgent demand for economical, effective, and reliable 3D hierarchically structured metal oxides that are capable of removing As(III). CuO is one of the most popular p-type semiconductor oxides. It has attracted much attention for its potential applications in lithium batteries, gas sensors, catalysts and field emission emitters.[32−38] Various CuO nanostructures have been used in removal of As(III) in water.[25,39] However, the adsorption capacities of these adsorbents for As(III) are relatively low (lower than 5 mg/g).[32,46] In addition, the mechanism of As(III) adsorption onto CuO was not clearly investigated. On the other hand, various CuO nanostructures with 3D hierarchical morphologies such as urchin-like, dandelion-like, cocoon-shaped and flower-shaped CuO have been fabricated by a series of solution-based routes.[25,30,40−42] To the best of our knowledge, the preparation

Received: November 28, 2011
Accepted: March 29, 2012
Published: March 29, 2012

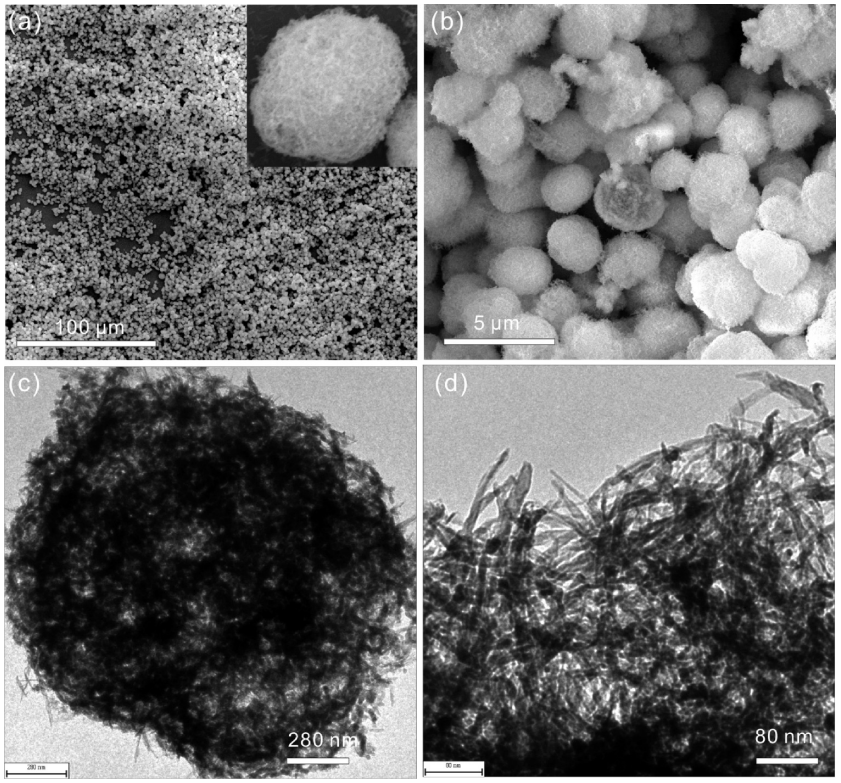

Figure 1. SEM images of the CuO precursor with (a) low and (b) high magnification; TEM image of the CuO precursor with (c) low and (d) high magnification; Cu^{2+}:urea = 1:3, T = 140 °C, and t = 12 h.

of 3D hierarchical cotton-candy-like CuO nanostructures has not been reported. In this study, a facile and surfactant-free solvothermal method was used to fabricate the novel porous cotton-candy-like CuO. The synthesized cotton-candy-like CuO microspheres were used for removal of As(III) with a higher adsorption capacity.

2. EXPERIMENTAL SECTION

Materials. Copper acetate monohydrate ($Cu(CH_3COO)_2{\cdot}H_2O$), urea, ethylene glycol (EG), ethanol, nitric acid (HNO_3), sodium hydroxide (NaOH), sodium sulfate (Na_2SO_4), sodium phosphate (Na_3PO_4), sodium carbonate (Na_2CO_3), sodium bicarbonate ($NaHCO_3$) and sodium chloride (NaCl) were all obtained from Sinopharm Chemical Reagent Co., Ltd., Shanghai, China. As(III) stock solution with a concentration of 1000 mg/L in HNO_3 medium was obtained from CANSPEC Co., Ltd., Shanghai, China. All chemicals were of analytical grade and used without further purification.

Synthesis of 3D Hierarchical cotton-candy-like CuO Precursor. In a typical synthesis, $Cu(CH_3COO)_2{\cdot}H_2O$ and urea with a molar ratio of 1:3 were dissolved and stirred in 100 mL of EG at room temperature until a homogeneous cloudy solution was formed. Then the homogeneous solution were transferred into a 125 mL Teflon-lined autoclave and heated at 140 °C for 12 h. After cooling to room temperature naturally, the solid precipitate was collected by centrifugation and washed three times with water and ethanol, respectively. The as-prepared green CuO precursors were dried at 60 °C for 12 h.

Synthesis of 3D Hierarchical cotton-candy-like CuO. The as-prepared precursor was placed into a muffle furnace and heated in air to 400 °C at a rate of 1 °C/min and maintained for 1 h. After the furnace was cooled to room temperature, the final black product was collected and kept for further characterization.

Characterization. Scanning electron microscopy (SEM) images were obtained with a FEI Quanta 200 FEG field emission scanning electron microscope. Transmission electron microscopy (TEM) and high-resolution TEM (HRTEM) analyses were performed using a JEM-2010 microscope. X-ray diffraction (XRD) was performed on a D/MaxIIIA X-ray diffractometer (Rigaku Co., Japan), using Cu Kα ($\lambda_{K\alpha1}$ = 1.5418 Å) as the radiation source. And the scan rate in the XRD measurement was 6.7 °/min. Thermogravimetric analysis (TGA) was performed on a SDT-Q600 DTG-TGA instrument. The Fourier transform infrared (FT-IR) spectra of the obtained samples were recorded with a NEXUS-870 FT-IR spectrometer in the range of 4000−400 cm^{-1}. X-ray photoelectron spectroscopy (XPS) analyses of the samples were conducted on a VG ESCALAB MKII spectrometer using an Mg Kα X-ray source (1253.6 eV, 120 W) at a constant analyzer. The Brunauer, Emmett and Teller (BET) specific surface areas were measured with a Micromeritics ASAP 2020 M analyzer. The As(III) concentrations were determined in the liquid phase using inductively coupled plasma atomic emission spectrometry (ICP-AES, Jarrell-Ash model ICAP 9000). pH value was measured using pH meter (Model: PHS-3C).

Adsorption Experiments. The rate of As(III) adsorption onto CuO was investigated by kinetics study. In the batch experiment the vials containing the adsorbent and solutions were vigorously agitated in order to eliminate external mass transport limitations; we determined the conditions for which external mass transfer limitation is no longer important, by varying the rate of agitation and measuring the corresponding rates of adsorption. An agitation speed of 200 rpm was deemed sufficient to eliminate external mass transport limitations, and all batch experiments were, therefore, carried out under such conditions. In the kinetics study of As(III) adsorption on CuO samples, the initial As(III) concentrations were 1 ppm. And the adsorbents dose was 0.4 g/L in the kinetics study. The pH values of the As(III) solutions were adjusted to 5.0 ± 0.2. And these samples were placed on a shaker for stirring. At predetermined time intervals, stirring was interrupted while 6 mL of supernatant solutions were pipetted and centrifuged for the determination of the remaining arsenic concentrations. For the equilibrium adsorption isotherm study, CuO with a loading of 0.5 g/L were added to As(III) solutions with different initial concentrations. Adsorption isotherms were used to

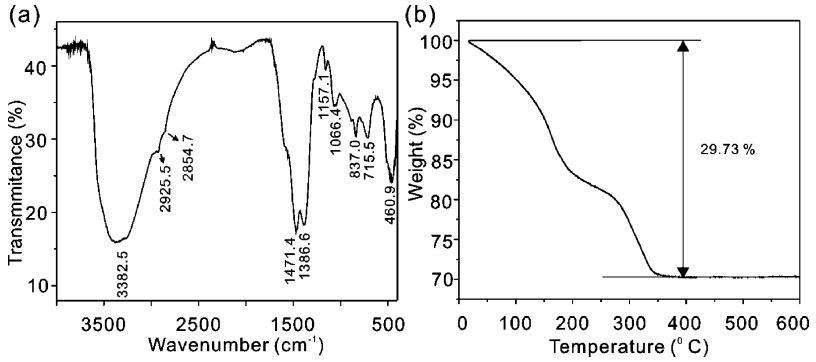

Figure 2. (a) FTIR spectra and (b) TGA curves of the as-obtained CuO precursor.

estimate the maximum adsorption capacity of CuO. Adsorption isotherms were investigated by using batch technique in polyethylene centrifuge tubes under ambient conditions. The pH values of all these As(III) solutions were also adjusted to 5.0 ± 0.2. For each point, these samples were mounted on the shaker for stirring 24 h. Our preliminary experiments found that 24 h was adequate for the suspension to obtain equilibrium. The adsorption capacity of the adsorbents for As(III) was calculated according to the following equation

$$q_e = \frac{(C_0 - C_e)V}{m} \quad (1)$$

where C_0 and C_e represent the initial and equilibrium As(III) concentrations (mg/L), respectively. V is the volume of the As(III) solution (mL), and m is the amount of adsorbent (mg).

To study the effects of competing anions, solutions were made by simultaneously adding As(III) and a single competing anion of interest. The competing anions in this study were phosphate, sulfate, carbonate, bicarbonate and chloride. Initial As(III) concentrations were 1 ppm and pH 5.0 ± 0.2. Competing anion concentrations were 30 ppm. The concentrations of the competing anions were chosen to be greater than the arsenic concentration in order to force competition for adsorption sites. The effect of pH on the adsorption of As(III) was studied by varying the initial pH of solutions between 3 and 11 and the initial As(III) concentration was 1 ppm.

The pH value was adjusted using 1 M HNO_3 and 1 M NaOH. All the adsorption experiments were carried out at room temperature (298 ± 2 K). All the experimental data were the average of triplicate determinations. The relative errors of the data were about 5%.

3. RESULTS AND DISCUSSION

The morphology of the CuO precursor was studied by SEM. The low-magnification SEM image (Figure 1a) demonstrates that the typical product consists of a large quantity of uniform microspheres. The inset of Figure 1a shows a single microsphere which reveals that the microsphere has cotton-candy-like nanostructures. The obtained cotton-candy-like nanostructures have a diameter of about 1−3 μm. The high-magnification SEM image of the cotton-candy-like nanostructures is shown in Figure 1b. See Figure S1 in the Supporting Information gives a typical broken microsphere. It can be seen from Figure S1 that the interior of the microspheres is composed of nanofibers. TEM observations further confirmed the result of the SEM. Figure 1c depicts the TEM image of an individual microsphere, from which we can see that the microspheres are highly porous and the nanofibers on the surface of the microsphere can be clearly seen. The TEM image in Figure 1d further reveals the edge of the microsphere is composed of interwoven nanofibers.

A series of other measurements were also used to investigate the as-obtained CuO precursor. The reaction between metal salts and EG and its product in the EG-mediated process have received considerable interests.[7,43−45] Although a variety of organometallic precursors produced from these processes have been investigated, however, detailed information on their crystal structures remain unclear and to determine the detailed structure of such a precursor is usually difficult.[45−47] The XRD pattern of the cotton-candy-like CuO precursor is shown in Figure S2 in the Supporting Information. The XRD pattern of CuO precursor in our study is very similar to the XRD patterns of SnO_2, In_2O_3, TiO_2, and PbO precursors in Xia et al's study where the metal oxide precursors were synthesized in EG.[43,44] The XRD pattern reported here could be assigned to a layered structure derived from the brucite structure according to Chakroune et al.[45] The main peaks in the XRD pattern were indexed as the (00l) reflections. And it was assumed that EG would lose its two protons and the dianion complexed with the metal center. Xia et al. has also studied the characteristically strong peak around 10 ° in a very similar polyol process.[43,44] It was considered to be a typical feature from the coordination and alcoholysis of EG with the center metal ions. According to Xia et al's study, the CuO precursor in our study is very possible to be copper glycolate. In the IR spectroscopic spectrum of the CuO precursor (Figure 2a), absorption peaks in the range of 1050−1500 cm^{-1} corresponding to $\rho(CH_2)$, $\nu(C-O)$ and $\nu(C-C)$ bands are observed. Absorptions were observed in the 2850−2950 cm^{-1} range, corresponding to ν_{as} and ν_s C−H bands. The adsorption peaks in the range of 400−850 cm^{-1} are associated with Cu−O, O−Cu−O, and Cu−O−Cu lattice vibrations. IR results are consistent with the XRD measurement. From the TG analysis (Figure 2b), a total weight loss of about 29.73% is observed because of the removal of organic species in the precursor by pyrolysis when the temperature was up to 400 °C. More work is underway to determine the detailed structure of such metal glycolate.

In the formation process of the cotton-candy-like CuO precursor microspheres, the ratio of Cu^{2+} to urea and the reaction temperature were found to play crucial roles. First, we studied the effect of the ratio of Cu^{2+} to urea on the morphology of the resultant products. In this experiment, the reaction temperature was fixed at 140 °C and the reaction time was fixed at 12 h. Figure S3 in the Supporting Information shows the SEM images of the products prepared at different Cu^{2+}/urea ratios. As shown in Figure S3a,b in the Supporting Information, only a small quantity of cotton-candy-like precursors are observed when the ratio of Cu^{2+} to urea was 1:4. When this ratio was increased to 1:5, some hollow CuO precursors can be seen (see Figure S3c,d in the Supporting Information). However, the hollow microspheres are not

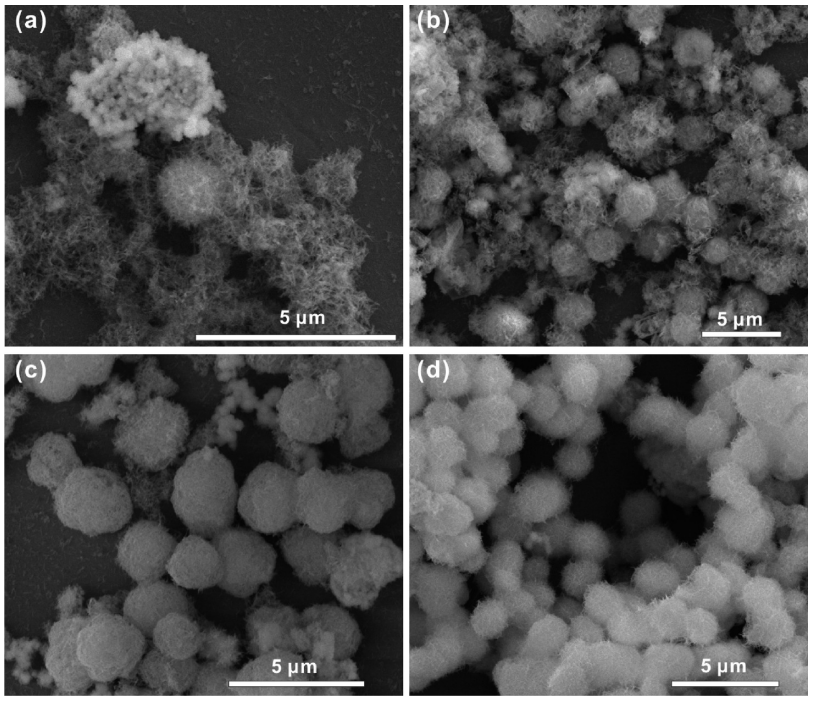

Figure 3. SEM images of the CuO precursor obtained at different times: (a) 40 min, (b) 2 h, (c) 8 h, and (d) 12 h.

uniform and there are a lot of fragments. The reaction temperature also has strong effects on the formation of the well-defined cotton-candy-like precursor. A series of samples were prepared after reaction at 120−180 °C for 12 h, while keeping the other experimental conditions unchanged. The SEM images (see Figure S4 in the Supporting Information) of the synthesized CuO precursors at different aging temperatures show very different morphologies from that of CuO precursor synthesized at 140 °C. CuO precursor prepared at 120 °C is consisted of some cotton-candy-like microspheres and some nanoparticles which were not assembled into microspheres. While the precursor prepared at 160 or 180 °C do not have organized structures. From the above analysis, we can conclude that the Cu^{2+}/urea ratio of 1:3 and the reaction temperature of 140 °C are essential for the synthesis of the cotton-candy-like CuO microspheres.

To study the morphological evolution of 3D hierarchical cotton-candy-like nanostructures, time-dependent experiments were done and products prepared at different growth stages were examined by SEM observation. As shown in Figure 3a, nanofibers were obtained at early stage (40 min) and some nanofibers have been assembled into some nanometer-sized sphere-like particles. Figure S5 gives the high resolution SEM image of a single particle of this kind, which clear shows that it is also composed of nanofibers. When the reaction time was prolonged to 2 h, Figure 3b shows some sphere-like particles has grown bigger and some of it has possessed micrometer-sized cotton-candy-like morphology accompanying by the decreasing number of nanofibers. As the reaction proceeded, the ratio of the cotton-candy-like nanostructures increased at the expense of nanofibers (Figure 3c). At the end, no nanometer-sized spherelike particles and nanofibers existed and the product was well-defined 3D cotton-candy-like nanostructure as shown in Figure 3d. EG has been used to fabricate mesostructures of titania, tin dioxide, zirconia, and niobium oxide by forming glycolate precursors because of its coordination ability with transition metal ions.[43] EG as complexing agent could coordinate with Cu^{2+} ions, which reduce the nucleation and growth rate of the precursors and prohibit them developing into bigger ones during the crystallization process. Xia et al. has used the EG-mediated method to synthesize 1D metal oxide nanowires.[43] They found that EG could serve as a ligand to form chain-like coordination complexes with Ti(IV), Sn(II), In(III), and Pb(II) cations upon heating.[43] The Cu(II) cations in our study are very possible to complex with EG to form chain-like coordination. As the chain-like complexes became sufficiently long, they would aggregate into bundles and the precipitate out from the reaction medium in the form of nanofibers which are made of the copper glycolate precursors. And then under external conditions such as electrostatic, nanofibers self-assembled and at a sufficiently high temperature (140 °C) and longer aging time, the micrometer-sized CuO precursor can be obtained.[16,24,48] On the other hand, we all know that above 80 °C urea can release CO_2 steadily which is responsible for the formation of highly porous structures of CuO precursors. On the basis of the above analysis, we proposed a two-stage growth process which involved a nucleation of amorphous primary nanofibers followed by the aggregation and self-assembly of nanofibers. The detailed formation mechanism for the final nanostructure by assembling primary particles is still a challenge in nanomaterial research. In addition, when EG was placed by H_2O, only irregularly shaped CuO precursors can be obtained (see Figure S6 in the Supporting Information).

To obtain CuO nanostructures, we must calcine the cotton-candy-like CuO precursor. Form the TG analysis (Figure 2b) we can see that 400 °C is enough to change the CuO precursors into CuO. And in our preliminary calcination experiments, we found that at longer duration time (more than 1 h) and higher temperature (more than 400 °C) the whole nanostructures were apt to collapse. So the CuO precursor in this study was calcined at 400 °C for 1 h in air and the green

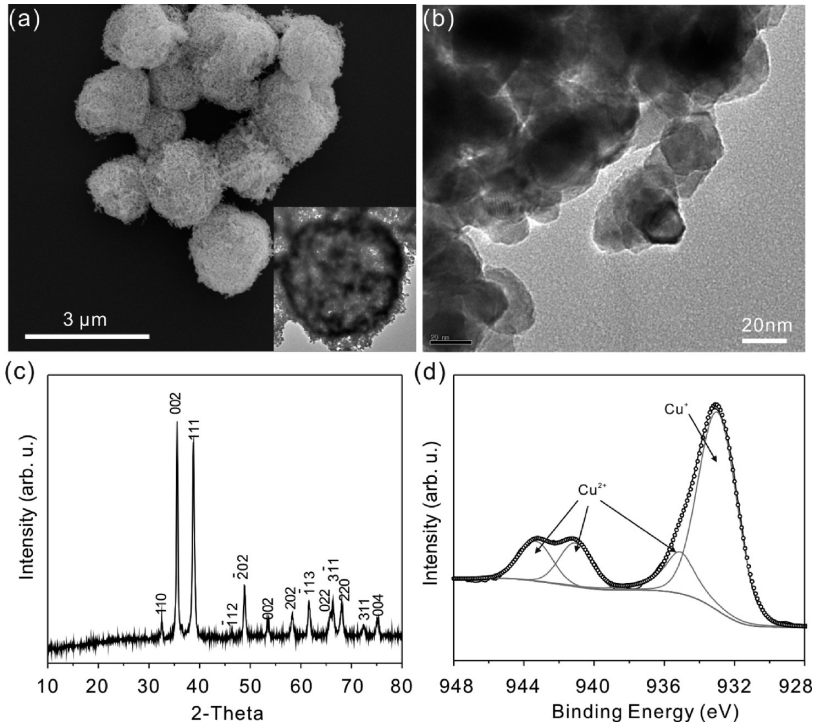

Figure 4. SEM images of the cotton-candy-like CuO with (a) low and (b) high magnification taken at the edge of the CuO nanostructures; Inset: a single TEM image of the cotton-candy-like CuO. (c) XRD pattern and (d) XPS characterization of the CuO nanostructures.

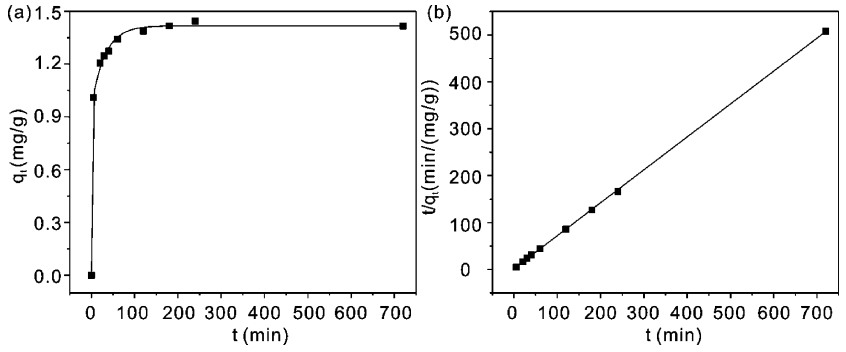

Figure 5. (a) Effects of contact time on the adsorption of As(III) onto cotton-candy-like CuO; (b) pseudo-second-order kinetic plots for the adsorption of As(III).

CuO precursors were changed to black CuO. Figure 4a shows the SEM image of the calcined product which implies that the calcination process dose not change the total cotton-candy-like morphology of the precursor. The inset of Figure 4a gives the TEM image of an individual CuO microsphere which confirms the result of SEM investigation. A high-resolution TEM image taken at the edge of the CuO microspheres (Figure 4b) shows that the surface has been changed from nanofibers of the CuO precursors to nanoparticles with a diameter about 20 nm. The measured spacing of the crystallographic planes is 0.25 and 0.27 nm (see Figure S7 in the Supporting Information), which corresponds to the (1 1 0) and (0 0 2) lattice fringe of the monoclinic CuO. The XRD pattern (Figure 4c) shows that the as-obtained sample after the calcination process is made of pure CuO which has the monoclinic symmetry (JCPDS Card No. 01−089−5895). No other impurities peaks are detected in the XRD pattern, indicating that the final product is pure. The surface of the as-prepared CuO microspheres was investigated by XPS. The XPS spectra of the Cu $2p_{3/2}$ core level and the shakeup satellites are shown in Figure 4d. Fits of the spectra show peaks at 933.0 and 935.1 eV. These two peaks are assigned to Cu^+ and Cu^{2+} core features, respectively. Peaks at 941.1 and 943.4 eV are assigned to Cu^{2+} satellites. The fitted curve for the O1s photoemission (see Figure S8 in the Supporting Information) exhibited three contributions. The peaks at 529.4 and 529.7 eV are assigned to CuO (curve 1) and Cu_2O (curve 2), respectively. And the peak at 531.3 eV (curve 3) can be assigned to hydroxyl groups. CuO in the XPS measurement conditions is apt to be reduced.[49] The cause of CuO reduction during the XPS measurement might be ascribed to exposure of the sample surface to electrons or photoelectrons from the X-ray window, photoreaction, thermal and electronic reactions, decomposition of hydrocarbon and the change of the surface composition in the ultrahigh vacuum system.[50−53] And the in situ reduction of CuO complicates quantification of the composition of copper oxide nanoparticles. As the XRD measurement (Figure 4c) confirms that the calcined products are pure phase CuO, we confirm that the

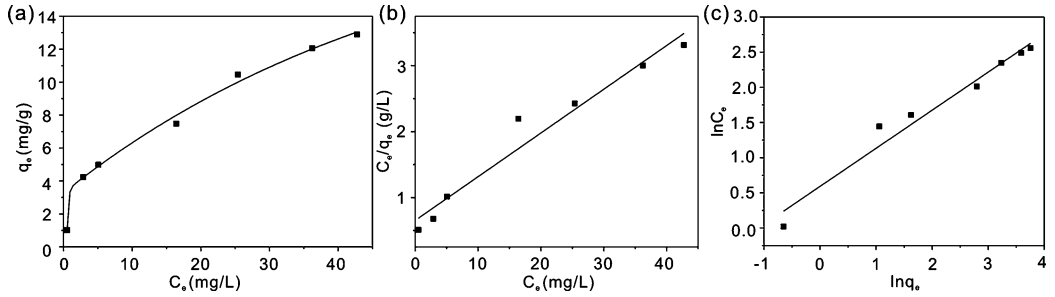

Figure 6. (a) Adsorption isotherms, linearized (b Langmuir) and (c) Freundlich isotherms of As(III) onto the cotton-candy-like CuO.

Cu^+ ions in the XPS measurement come from the reduction of Cu^{2+} in CuO. Similar results have also been reported in many other literatures.[49−53] Survey scans of the CuO sample reveals that the ratio of O to Cu is about 1.3, which is believed to be caused by O in the adventitious carbohydrates adsorbed on the CuO sample during the handling of XPS measurement.

The kinetics of adsorption, which describes the solute uptake rate governing the residence time of the adsorption reaction, is one of the most important characteristics that define the efficiency of adsorption. The kinetics of As(III) adsorption onto cotton-candy-like CuO is shown in Figure 5a. It is clear from Figure 5a that the adsorption rate of As(III) is rather fast. The adsorption of As(III) is rapid at first and then slows considerably. On the basis of the specific nanostructures of the cotton-candy-like CuO and the adsorption rate, the adsorption model is proposed in our study. That is: arsenic is initially adsorbed by CuO nanoparticles on the exterior surface of the CuO microspheres. When the adsorption at the exterior surface reaches the saturation level, the arsenic begin to enter the exterior via the pores and move into the interior of the CuO microspheres adsorbed by the nanoparticles nearest to the exterior of the microspheres, and at last adsorbed by the interior nanoparticles. When arsenic ion diffuse into the interior of the CuO microspheres, the diffusion resistance is increased; this in turn leads to a decrease in diffusion rate. And the exterior followed by interior sorption model has been fully evidenced by the adsorption rate in the adsorption kinetics study. In such experimental conditions, most of As(III) could be removed after 2 h. In addition, the above adsorption kinetic experimental data can be best fitted into a pseudo-second-order rate kinetic model. The pseudo-second-order model is presented as follows:[54]

$$\frac{t}{q_t} = \frac{1}{k_2 q_e^2} + \frac{1}{q_e} t \tag{2}$$

where k_2 is the rate constant of the pseudo-second-order model of adsorption (g/mg/min). q_t is the amount of As(III) adsorbed on the surface of the adsorbent at time t, and q_e is the equilibrium adsorption capacity which is a calculated value. For the pseudo-second-order model, the values of k_2 and q_e can be obtained by a plot of t/q_t against t. The pseudo-second-order kinetics plot for the adsorption of As(III) onto cotton-candy-like CuO samples is shown in Figure 5b. Figure 5b demonstrates that the experimental data could be well fitted with the linear form of the pseudo-second-order model. The correlation coefficient value for pseudo-second-order model is 0.99986 (Tab.S1), suggesting that the pseudo-second-order model best represents the adsorption kinetics in our adsorbent systems. And we also found that the value of calculated q_e was very close to that of experimental q_e.

The adsorption capacity of cotton-candy-like CuO for As(III) was evaluated using the equilibrium adsorption isotherm by varying the initial As(III) concentrations. Figure 6a shows the adsorption isotherms of As(III) onto cotton-candy-like CuO at room temperature. From Figure 6a we can see that the adsorption capacity of the cotton-candy-like CuO for As(III) does not reach the adsorption saturation and it could increase further with the increase in the equilibrium As(III) concentration. The experiment result here shows that the adsorption capacity of these CuO microspheres should be larger than 12.9 mg/g. Two empirical equations Langmuir and Freundlich isotherms models were used to analyze the experimental data. The mathematical expressions of the Langmuir isotherm and the Freundlich isotherms model are:[54,55]

$$\frac{C_e}{q_e} = \frac{1}{q_m K_L} + \frac{C_e}{q_m} \tag{3}$$

$$\ln q_e = \frac{1}{n} \ln C_e + \ln K_F \tag{4}$$

where q_m and K_L are Langmuir constants, representing the maximum adsorption capacity of adsorbents (mg/g) and the energy of adsorption, respectively. K_F and n are Freundlich constants related to adsorption capacity and adsorption intensity, respectively.

The linearized Langmuir isotherms and Freundlich isotherms of As(III) onto cotton-candy-like CuO are presented in Figure 6b,c, respectively. The parameters of the Langmuir and Freundlich models were calculated and listed in Table S2 in the Supporting Information. From the correlation coefficients, it can be seen that the adsorption data for As(III) onto cotton-candy-like CuO fit the Freundlich isotherm model better than the Langmuir isotherm model. To assess the As(III) removal performance of cotton-candy-like CuO samples, the adsorption capacity of the samples for As(III) was compared with other nanostructured CuO materials (Table 1). Table 1 indicates that the adsorption capacity of cotton-candy-like CuO for As(III) in this study is higher than that of the other 3D hierarchical CuO

Table 1. Adsorption Capacity Comparisons of Cotton-Candy-Like CuO in This Study with Other Structured CuO Adsorbents for Removal of As(III)

adsorbents	adsorption capacity (mg/g)	ref
cotton-candy-like CuO	>12.9	this study
Doughnut-like CuO	4.7	25
CuO nanoparticles	1.4	25
CuO incorporated mesoporous alumina	2.16	39

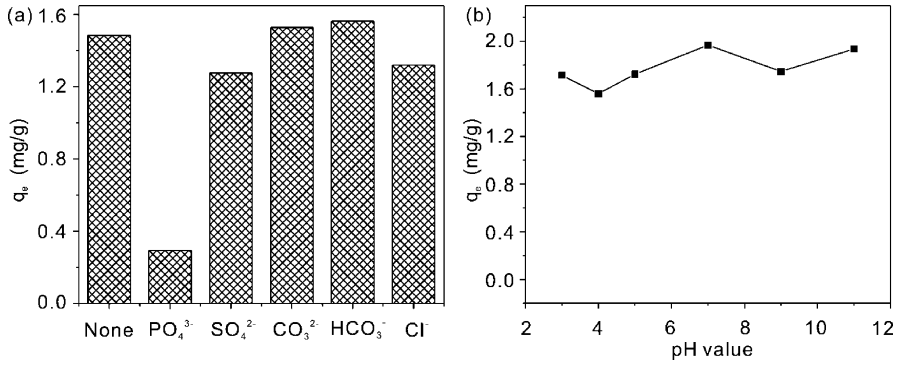

Figure 7. Effects of (a) competing anions and (b) pH value on adsorption of As(III) onto the cotton-candy-like CuO.

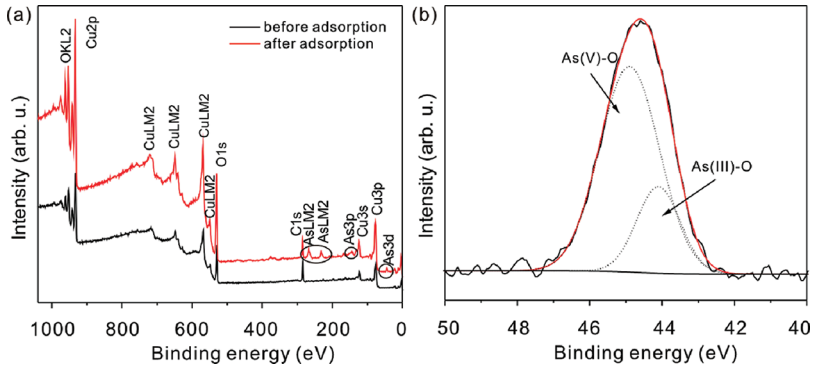

Figure 8. (a) XPS wide scan of the cotton-candy-like CuO before and after adsorption of As(III). (b) High-resolution As3d spectra of the cotton-candy-like CuO after adsorption of As(III).

nanostructures, CuO nanoparticles and CuO nanoparticles impregnated materials. For instance, the adsorption capacity of doughnut-like CuO for As(III) is just 4.7 mg/g, whereas for cotton-candy-like CuO in this study, the adsorption capacity for As(III) is higher than 12.9 mg/g. In order to explain the better adsorption capacity of cotton-candy-like CuO compared with other nanostructured CuO, the BET surface area measurement was done. The BET surface area of the cotton-candy-like CuO is 119 m^2/g which is higher than CuO nanoparticles (27 m^2/g)[25] and doughnut-like CuO (87 m^2/g)[25] and lower than CuO incorporated mesoporous alumina (189.25 m^2/g).[39] The higher BET surface area of the cotton-candy-like CuO microspheres than CuO nanoparticles and doughnut-like CuO may be one of the reasons that lead to their higher adsorption capacity. The larger specific surface area of the cotton-candy-like nanostructures benefits from its 3D hierarchical highly porous structure making its inner nanometer-sized nanoparticles and pores easily accessible. As to CuO incorporated mesoporous alumina, the higher BET surface area is mainly due to the high surface area of mesoporous alumina. Although the CuO incorporated mesoporous alumina have higher surface area than other nanostructured CuO, the per unit area of CuO loading is lower than that of CuO nanoparticles, doughnut-like CuO and cotton-candy-like CuO. On the other hand, it has been reported that the hydroxyl group on the surface of metal oxide are responsible for the adsorption of arsenic.[56] In the XPS analysis we have showed that there are plenty hydroxyl groups on the surface of cotton-candy-like CuO. However, we can not find the reported data for the number of hydroxyl groups in the literatures about CuO nanoparticles and doughnut-like CuO. So we can not compare this data with others. In brief, we believe that the higher adsorption capacity is due to the novel porous 3D hierarchical nanostructures (higher specific surface area) and more surface hydroxyl groups of the cotton-candy-like CuO.

To study the effect of coexisting anions such as phosphate, sulfate, chloride, carbonate, and bicarbonate, which compete in adsorption process, the adsorption studies were carried out in the presence of these anions. The initial concentration of As(III) was maintained at 1 ppm and the concentrations of phosphate, sulfate, chloride, carbonate, and bicarbonate were all 30 ppm. The effect of these anions on As(III) removal is presented in Figure 7a. It is observed that removal of As(III) is not marginally affected by the presence of these anions except phosphate. This means that the cotton-candy-like CuO has relatively higher affinity for As(III) as compared to anions namely sulfate, chloride, carbonate and bicarbonate which are commonly encountered in groundwater. It has been reported that the adsorption of As(III) on metal oxides is through formation of inner-sphere surface complexes which are mainly attached as bidentate linkages with some monodentate linkages.[57] Also, it has been reported that adsorption following the formation of inner sphere complexes are not much influenced by pH.[58] Removal of As(III) by cotton-candy-like CuO is less influenced at different pH (which will be shown in the following study) which also indicates that the adsorption of As(III) on cotton-candy-like CuO is through formation of inner sphere complex through formation of As−O linkages. So cotton-candy-like CuO has higher affinity for As(III) compared to other anions. The removal of As(III) from water is highly dependent on pH and it has been observed that for most of the adsorbents adsorption capacity changes drastically with variation in pH. To study the effect of pH on As(III) adsorption capacity of cotton-candy-like CuO, As(III) removal

was studied at pH ranging between 3 and 11. As evident from Figure 7b, there is only slight variation in the As(III) removal with variation in pH. This indicates that cotton-candy-like CuO can be used in a wide range of pH environments for removal of As(III). In addition, the CuO samples can be regenerated by rinsing with 0.5 M NaOH solution. More than 90% As(III) can be desorbed from the CuO nanostructures. Especially, after 5 cycles of reuse, the adsorption capacity of CuO nanostructures can still maintain 80% that of the fresh cotton-candy-like CuO. However, to evaluate the performance of the CuO adsorbent, we must test some practical polluted water, and these experiments are ongoing.

To investigate the adsorption mechanism of As(III) onto cotton-candy-like CuO samples, the chemical status of As(III) species after their adsorption onto CuO samples was investigated by XPS over the adsorbent surface (Figure 8). Compared with raw CuO, there are four obvious peaks of arsenic (As3d core level peak as well as AsLM2 and As3p peaks) in the wide-scan spectra of CuO after adsorption of As(III), which confirms the presence of arsenic (Figure 8a). High-resolution XPS spectra of the As3d peak are shown in Figure 8b. The fitted curve for the As3d photoemission exhibited two contributions. The peaks at 44.10 and 44.90 eV are assigned to As(III)-O and As(V)-O, respectively. This reveals that some As(III) on the surface of the CuO microspheres have been oxidized to As(V) which is less toxic than As(III) and the CuO microspheres also have adsorption affinity for As(V). The oxidation properties of CuO have been intensively investigated.[37] For example, copper oxide materials have been found to be effective catalysts for CO and NO oxidation as well as oxidation of volatile organic chemicals such as methanol.[59,60] In addition, previous experimental results have shown that there are hydroxyl groups on the surface of the CuO microspheres (see Figure S7 in the Supporting Information). The surface hydroxyl groups on the metal oxides have been demonstrated to be responsible for the effective adsorption of both As(III) and As(V) in water.[56] The above analysis suggested that the adsorption of As(III) onto CuO samples is not a simple and single process. The whole adsorption process involves the adsorption of As(III) onto CuO and the oxidation of As(III) to As(V) followed by adsorption of As(V) onto CuO samples. This oxidation and sorption mechanism could well explain the higher As(III) uptake capacity. However, as the particle size of these CuO nanoparticles is small (1−3 μm), the use of nano adsorbents needs to combine with other conventional techniques in a practical situation for remediating a polluted groundwater. For example, we can immobilize the CuO nanostructures onto activated carbon fiber or other supporters and combine the CuO adsorbents with nanofiltration to prevent the CuO nanostructures from releasing into the cleaned water.

4. CONCLUSIONS

Novel cotton-candy-like CuO 3D hierarchical microspheres were successfully synthesized by a facile surfactant-free solvothermal route and subsequent calcination process. The investigations show that the ratio of Cu^{2+} to urea, the reaction temperature and the use of EG play important roles in the formation of the cotton-candy-like CuO precursor. The possible formation mechanism was also proposed. As(III) adsorption experiments indicated that the as-synthesized CuO hierarchical nanostructures exhibited fast adsorption rates and higher removal capacity than other reported nanostructured CuO adsorbents. The presence of most of the competing anions in water did not inhibit the adsorption of As(III) onto the cotton-candy-like CuO microspheres. And in a wide range of pH value, the adsorption capacity of CuO samples for As(III) changed little. The XPS results show that the whole adsorption procedure of As(III) onto CuO is an oxidation coupled with sorption approach. The above results suggest that the cotton-candy-like CuO microspheres are an effective material for As(III) adsorption and may be used to develop a simple and efficient As(III) removal method.

■ ASSOCIATED CONTENT

Supporting Information

High-resolution SEM image of a broken CuO microsphere; XRD pattern of the CuO precursor; SEM images of the samples with different ratios of Cu^{2+} to urea; SEM images of the samples prepared at different temperature; High resolution SEM image of the CuO spherelike particle; SEM images of the samples prepared in pure water; HRTEM image of CuO nanoparticles on the edge of the cotton-candy-like CuO microspheres; O1s core level spectra of the CuO nanostructures; Kinetics parameters of As(III) adsorption onto the cotton-candy-like CuO; Equilibrium adsorption isotherm fitting parameters for As(III) onto cotton-candy-like CuO. This material is available free of charge via the Internet at http://pubs.acs.org/.

■ AUTHOR INFORMATION

Corresponding Author

*E-mail: xingjiuhuang@iim.ac.cn. Tel.: +86-551-5591142. Fax: +86-551-5592420.

Author Contributions

§These two authors contributed equally to this work.

Notes

The authors declare no competing financial interest.

■ ACKNOWLEDGMENTS

This work was supported by the One Hundred Person Project of the Chinese Academy of Sciences, China, the National Key Scientific Program-Nanoscience and Nanotechnology (No. 2011CB933700), National Natural Science Foundation of China (Grant 21103198 and 60801021) and the China Postdoctoral Science Foundation (20110490386 and 2011M501073).

■ REFERENCES

(1) Zhang, J.; Sun, L. D.; Yin, J. L.; Su, H. L.; Liao, C. S.; Yan, C. H. *Chem. Mater.* **2002**, *14*, 4172.
(2) Li, X. Y.; Si, Z. J.; Lei, Y. Q.; Li, X. N.; Tang, J. K.; Song, S. Y.; Zhang, H. J. *CrystEngComm* **2011**, *13*, 642.
(3) Xu, L.; Lu, C. L.; Zhang, Z. H.; Yang, X. Y.; Hou, W. H. *Nanoscale* **2010**, *2*, 995.
(4) Zhou, W. J.; Liu, X. Y.; Cui, J. J.; Liu, D.; Li, J.; Jiang, H. D.; Wang, J. Y.; Liu, H. *CrystEngComm* **2011**, *13*, 4557.
(5) Zhu, Y. C.; Mei, T.; Wang, Y.; Qian, Y. T. *J. Mater. Chem.* **2011**, *21*, 11457.
(6) Xiao, W.; Wang, D. L.; Lou, X. W. *J. Phys. Chem. C* **2010**, *114*, 1694.
(7) Cao, A. M.; Hu, J. S.; Liang, H. P.; Song, W. G.; Wan, L. J.; He, X. L.; Gao, X. G.; Xia, S. H. *J. Phys. Chem. B* **2006**, *110*, 15858.
(8) Dong, W. J.; Wang, X. B.; Li, B. J.; Wang, L. N.; Chen, B. Y.; Li, C. R.; Li, X. A.; Zhang, T. R.; Shi, Z. *Dalton Trans.* **2011**, *40*, 243.

(9) Li, Y. Y.; Liu, J. P.; Huang, X. T.; Li, G. Y. *Cryst. Growth Des.* **2007**, *7*, 1350.
(10) Li, Y.; Cao, M. H.; Feng, L. Y. *Langmuir* **2009**, *25*, 1705.
(11) Sun, Y. G.; Zou, R. J.; Tian, Q. W.; Wu, J. H.; Chen, Z. G.; Hu, J. Q. *CrystEngComm* **2011**, *13*, 2273.
(12) Sun, C. W.; Rajasekhara, S.; Goodenough, J. B.; Zhou, F. *J. Am. Chem. Soc.* **2011**, *133*, 2132.
(13) Li, X. A.; Zhang, B.; Ju, C. H.; Han, X. J.; Du, Y. C.; Xu, P. *J. Phys. Chem. C* **2011**, *115*, 12350.
(14) Sun, P.; Zhao, W.; Cao, Y.; Guan, Y.; Sun, Y. F.; Lu, G. Y. *CrystEngComm* **2011**, *13*, 3718.
(15) Wang, W. S.; Hu, Y. X.; Goebl, J.; Lu, Z. D.; Zhen, L.; Yin, Y. D. *J. Phys. Chem. C* **2009**, *113*, 16414.
(16) Zhong, L. S.; Hu, J. S.; Liang, H. P.; Cao, A. M.; Song, W. G.; Wan, L. J. *Adv. Mater.* **2006**, *18*, 2426.
(17) Cai, W. Q.; Yu, J. G.; Jaroniec, M. *J. Mater. Chem.* **2010**, *20*, 4587.
(18) Li, H.; Li, W.; Zhang, Y. J.; Wang, T. S.; Wang, B.; Xu, W.; Jiang, L.; Song, W. G.; Shu, C. Y.; Wang, C. R. *J. Mater. Chem.* **2011**, *21*, 7878.
(19) Cao, S. W.; Zhu, Y. J. *J. Phys. Chem. C* **2008**, *112*, 6253.
(20) Hu, J. S.; Zhong, L. S.; Song, W. G.; Wan, L. J. *Adv. Mater.* **2008**, *20*, 2977.
(21) Cai, W. Q.; Yu, J. G.; Cheng, B.; Su, B. L.; Jaroniec, M. *J. Phys. Chem. C* **2009**, *113*, 14739.
(22) Mou, F. Z.; Guan, J. G.; Xiao, Z. D.; Sun, Z. G.; Shi, W. D.; Fan, X. A. *J. Mater. Chem.* **2011**, *21*, 5414.
(23) Fei, J. B.; Cui, Y.; Zhao, J.; Gao, L.; Yang, Y.; Li, J. B. *J. Mater. Chem.* **2011**, *21*, 11742.
(24) Zhong, L. S.; Hu, J. S.; Cao, A. M.; Liu, Q.; Song, W. G.; Wan, L. J. *Chem. Mater.* **2007**, *19*, 1648.
(25) Cao, A. M.; Monnell, J. D.; Matranga, C.; Wu, J. M.; Cao, L. L.; Gao, D. *J. Phys. Chem. C* **2007**, *111*, 18624.
(26) Amini, M.; Abbaspour, K. C.; Berg, M.; Winkel, L.; Hug, S. J.; Hoehn, E.; Yang, H.; Johnson, C. A. *Environ. Sci. Technol.* **2008**, *42*, 3669.
(27) Mohan, D.; Pittman, C. U. *J. Hazard. Mater.* **2007**, *142*, 1.
(28) Manning, B. A.; Hunt, M. L.; Amrhein, C.; Yarmoff, J. A. *Environ. Sci. Technol.* **2002**, *36*, 5455.
(29) Manning, B. A.; Goldberg, S. *Environ. Sci. Technol.* **1997**, *31*, 2005.
(30) Lee, H.; Choi, W. *Environ. Sci. Technol.* **2002**, *36*, 3872.
(31) Kim, Y. H.; Kim, C. M.; Choi, I. H.; Rengaraj, S.; Yi, J. H. *Environ. Sci. Technol.* **2004**, *38*, 924.
(32) Zou, G. F.; Li, H.; Zhang, D. W.; Xiong, K.; Dong, C.; Qian, Y. T. *J. Phys. Chem. B* **2006**, *110*, 1632.
(33) Liu, Y. L.; Liao, L.; Li, J. C.; Pan, C. X. *J. Phys. Chem. C* **2007**, *111*, 5050.
(34) Chen, J.; Deng, S. Z.; Xu, N. S.; Zhang, W. X.; Wen, X. G.; Yang, S. H. *Appl. Phys. Lett.* **2003**, *83*, 746.
(35) Gao, S. Y.; Yang, S. X.; Shu, J.; Zhang, S. X.; Li, Z. D.; Jiang, K. *J. Phys. Chem. C* **2008**, *112*, 19324.
(36) Zhang, J. T.; Liu, J. F.; Peng, Q.; Wang, X.; Li, Y. D. *Chem. Mater.* **2006**, *18*, 867.
(37) Xu, L. P.; Sithambaram, S.; Zhang, Y. S.; Chen, C. H.; Jin, L.; Joesten, R.; Suib, S. L. *Chem. Mater.* **2009**, *21*, 1253.
(38) Anandan, S.; Wen, X. G.; Yang, S. H. *Mater. Chem. Phys.* **2005**, *93*, 35.
(39) Pillewan, P.; Mukherjee, S.; Roychowdhury, T.; Das, S.; Bansiwal, A.; Rayalu, S. *J. Hazard. Mater.* **2011**, *186*, 367.
(40) Deng, C. H.; Hu, H. M.; Zhu, W. L.; Han, C. L.; Shao, G. Q. *Mater. Lett.* **2011**, *65*, 575.
(41) Vaseem, M.; Umar, A.; Kim, S. H.; Hahn, Y. B. *J. Phys. Chem. C* **2008**, *112*, 5729.
(42) Manna, S.; Das, K.; De, S. K. *ACS Appl. Mater. Interfaces* **2010**, *2*, 1536.
(43) Jiang, X. C.; Wang, Y. L.; Herricks, T.; Xia, Y. N. *J. Mater. Chem.* **2004**, *14*, 695.
(44) Wang, Y. L.; Jiang, X. C.; Xia, Y. N. *J. Am. Chem. Soc.* **2003**, *125*, 16176.
(45) Chakroune, N.; Viau, G.; Ammar, S.; Jouini, N.; Gredin, P.; Vaulay, M. J.; Fievet, F. *New J. Chem.* **2005**, *29*, 355.
(46) Larcher, D.; Sudant, G.; Patrice, R.; Tarascon, J. M. *Chem. Mater.* **2003**, *15*, 3543.
(47) Poul, L.; Jouini, N.; Fievet, F. *Chem. Mater.* **2000**, *12*, 3123.
(48) Politi, Y.; Arad, T.; Klein, E.; Weiner, S.; Addadi, L. *Science* **2004**, *306*, 1161.
(49) Wu, C. K.; Yin, M.; O'Brien, S.; Koberstein, J. T. *Chem. Mater.* **2006**, *18*, 6054.
(50) Wallbank, B.; Johnson, C. E.; Main, I. G. *J. Electron. Spectrosc.* **1974**, *4*, 263.
(51) Arko, A. J.; List, R. S.; Bartlett, R. J.; Cheong, S. W.; Fisk, Z.; Thompson, J. D.; Olson, C. G.; Yang, A. B.; Liu, R.; Gu, C.; Veal, B. W.; Liu, J. Z.; Paulikas, A. P.; Vandervoort, K.; Claus, H.; Campuzano, J. C.; Schirber, J. E.; Shinn, N. D. *Phys. Rev. B* **1989**, *40*, 2268.
(52) Losev, A.; Kostov, K.; Tyuliev, G. *Surf. Sci.* **1989**, *213*, 564.
(53) Klein, J. C.; Chung, P. L.; Hercules, D. M.; Black, J. F. *Appl. Spectrosc.* **1984**, *38*, 729.
(54) Yu, X. Y.; Luo, T.; Zhang, Y. X.; Jia, Y.; Zhu, B. J.; Fu, X. C.; Liu, J. H.; Huang, X. J. *ACS Appl. Mater. Interf.* **2011**, *3*, 2585.
(55) Li, Y. H.; Liu, F. Q.; Xia, B.; Du, Q. J.; Zhang, P.; Wang, D. C.; Wang, Z. H.; Xia, Y. Z. *J. Hazard. Mater.* **2010**, *177*, 876.
(56) Xu, Z. C.; Li, Q.; Gao, S. A.; Shang, J. K. *Water Res.* **2010**, *44*, 5713.
(57) Goldberg, S.; Johnston, C. T. *J. Colloid Interface Sci.* **2001**, *234*, 204.
(58) Maliyekkal, S. M.; Philip, L.; Pradeep, T. *Chem. Eng. J.* **2009**, *153*, 101.
(59) Ratnasamy, P.; Srinivas, D.; Satyanarayana, C. V. V; Manikandan, P.; Kumaran, R. S. S.; Sachin, M.; Shetti, V. N. *J. Catal.* **2004**, *221*, 455.
(60) Purnama, H.; Ressler, T.; Jentoft, R. E.; Soerijanto, H.; Schlogl, R.; Schomacker, R. *Appl. Catal. A* **2004**, *259*, 83.